Moisture Transport in Shrinking Gels during Saturated Drying

Srinivas Achanta
Process Systems Technology, The Procter & Gamble Company, Cincinnati, OH 45232

Martin R. Okos
Dept. of Agricultural and Biological Engineering, Purdue University, West Lafayette, IN 47907

John H. Cushman
Center for Applied Mathematics, Mathematical Sciences Building, Purdue University, West Lafayette, IN 47907

David P. Kessler
School of Chemical Engineering, Purdue University, West Lafayette, IN 47907

The transport of moisture in shrinking food gels during drying is studied based on a novel thermomechanical theory accounting for a structural transition in the material — from the rubbery to the glassy state — during drying. The proposed theory is applied to the drying of a model cylindrical starch – gluten gel system. The predicted drying characteristics depend on the Deborah number, a ratio of the characteristic relaxation time to the characteristic diffusion time. At low Deborah numbers, drying is Fickian. At intermediate and high Deborah numbers, however, drying is non-Fickian, leading to an apparent mass-transfer shutdown, which is a result of surface dryout and skin/shell formation. Based on a time-dependent surface boundary condition, the model proposes that surface drying is not only a function of the Biot number but also a function of the "Shell" number, a ratio of the Deborah and Biot numbers. The model is verified by comparing its predictions with experimental data from drying of starch – gluten gels at 22.5 and 40°C. The model predictions agree with experimental data and capture the observed sigmoidal shape of the experimental drying curves in the saturated flow regime. The predicted moisture profiles show shell formation and growth during drying, compatible with the experimental moisture profiles from the literature.

Introduction

Drying of high-moisture biopolymers such as processed foods, gels, fruits, and vegetables occurs predominantly in the saturated flow regime, where shrinkage almost entirely compensates for the loss of water. As shown by Jomaa and Puiggali (1991) for cellulosic gels, Lartigue et al. (1989) for wood, Ketelaars et al. (1992) for clays, Karathanos et al. (1993) for celery, and Crapiste et al. (1985) and Suarez and Viollaz (1991) for potato slabs, drying of high-moisture food biological materials results in a bulk-density change that is linearly related to the change in product moisture content. Hence, accounting for shrinkage in a mechanistic or mathematical model of the drying of biological materials is important. Several models exist in the literature that account for matrix shrinkage during drying, either analytically (Viollaz, 1985) or numerically by using finite difference (Crapiste et al., 1985) or finite-element formulation (Ketelaars et al., 1992). These and other related works provide a good understanding of volume/density changes during drying and serve as better models for drying of biological materials than those models that do not account for shrinkage. However, they are still incomplete because they generally are empirical in nature and neglect the nonequilibrium characteristics of shrinkage.

Correspondence concerning this article should be addressed to M. R. Okos.

Swelling and shrinkage in high-molecular-weight polymers are not elastic but a viscoelastic (time-dependent) nonequilibrium phenomenon (Ferry, 1980). As shown by Kishimoto et al. (1960), solvent absorption by glassy polymers—the inverse of a solvent desorption or drying process—is non-Fickian and the sorption process is two stage. This anomalous sorption process, also referred to as Case II diffusion in the polymer literature (Peppas and Korsmeyer, 1987), is due to matrix viscous swelling during sorption (Thomas and Windle, 1982). Thomas and Windle (1982) incorporated viscous swelling effects in their solvent-transport equation, and successfully predicted the Case II diffusion process.

The semiempirical approach of Thomas and Windle (1982) is, however, incomplete in that they assume that solvent uptake is controlled by an effective diffusivity, an empirical parameter that lumps the effects of (a) various matrix properties such as porosity, pore tortuosity, and pore connectivity; and (b) solvent properties such as viscosity. This approach hence cannot provide a fundamental understanding of the sorption process. This limitation arises because this approach considers the liquid and the matrix as a single-phase mixture, an assumption that is unrealistic because the mixture is in fact multiphase. Further, Thomas and Windle (1982) intuitively postulated and did not derive their viscous swelling relation. The limitations of this approach may be overcome by applying Darcy's law, which treats the polymer–solvent system as a multiphase matrix and not as a homogeneous mixture. The multiphase transport theories such as the volume-averaging approach of Whitaker (1980) provide a stronger theoretical base to model this transport process.

Whitaker (1980) pioneered the application of the volume-averaging approach to drying. This theory treats the drying problem as a multiphase transport problem, but is valid only for nondeforming granular systems, since it is based on the conventional Darcy's law that does not account for viscoelastic deformations during drying. Hence this drying theory cannot explain the anomalous moisture profiles measured experimentally by either Litchfield and Okos (1992) during drying of pasta or Schrader and Litchfield (1992) during drying of gels. To overcome the drawbacks of Whitaker's model, Achanta et al. (1994) used the hybrid-mixture theory to modify the Darcy's law to suit viscoelastic deforming materials. As shown by Achanta and Cushman (1994), the hybrid mixture theory can also provide a derivation for the viscosity-based deformation relation of Thomas and Windle (1982). The current work incorporates the viscosity-based deformation relation in the Darcy's law framework to derive the overall moisture transport equation that overcomes the limitations of the theories proposed by Thomas and Windle (1982) and Whitaker (1980). The predicted drying characteristics depend on the Deborah number, a ratio of the characteristic relaxation time to the characteristic diffusion time. Based on a time-dependent surface boundary condition, the model proposes that surface drying is not only a function of the Biot number but also a function of the "Shell" number, a ratio between the Deborah and Biot numbers. The model is also verified by comparing its predictions with experimental data from drying of starch–gluten gels at 22.5°C and 40°C. This model provides the basis for further investigation of phenomena such as case-hardening and stress-cracking during drying of food and polymeric materials.

Model Development

Mechanistic description of transport mechanisms during food biopolymer drying

To understand the quality changes that occur in foods during drying, it is not only important to identify the mechanism of moisture transport but also the associated changes in the material during different stages of drying. Most bipolymers, including foodstuffs, are dried from high moistures where collapse can be significant to very low moistures where collapse is generally negligible (at least in time scales of interest to the processor). For example, vegetable drying typically occurs from a moisture content of 2,000% (dry basis) to 15% (Karathanos et al., 1993). Another example is that of pasta drying, where moisture changes from 35% to 5% (Waananen and Okos, 1991).

The consequences of drying from high to low moistures are twofold. First, the material, which is initially of a rubbery texture, is transformed to a brittle texture. Second, the moisture transport in the material, which is dominated by liquid-phase transport initially, may change predominantly to the vapor phase at low moistures. The transformations in the texture of the material and in the mechanism of moisture transport in the material are interrelated. At high moistures, when the material has a rubbery texture, shrinkage almost entirely compensates for moisture loss. As moisture content decreases the rate of shrinkage decreases drastically since the material becomes more elastic. At this point, further moisture loss is not compensated by shrinkage and pore-space formation in the material starts. Further drying diminishes the dominance of liquid flow, and eventually vapor flow dominates (Waananen and Okos, 1991).

Another important aspect of drying biopolymers is the rate at which the material is dried. A biopolymer at high moisture will collapse at a certain rate during drying, depending on local moisture and temperature. This collapse rate, which is an inherent viscoelastic characteristic of the biopolymer, is a function of the difference between the T_g and the temperature of drying. At high moistures, collapse occurs at a faster rate than at low moistures. Hence if a high-moisture-content material is greatly above the T_g and is subjected to rapid drying conditions (high temperatures and low relative humidities), the surface collapses at a rate comparable to the rate at which moisture diffuses from the interior to the surface, and the material forms a dense crust or shell. In other words, if dense-shell formation occurs when the material surface is maintained above its T_g, the material collapses to make up for the lost volume of water. From the moisture profile standpoint, a shell or crust may be defined as that region in the material where steep moisture gradients persist during drying. The formation of a shell during drying of gels was verified experimentally by Schrader and Litchfield (1992).

If a high-moisture-content material is dried at a slow rate (low temperatures and high relative humidities) so that moisture gradients are negligible, the rate of drying is comparable to the rate of collapse and the time-scale available for moisture diffusion from the interior to the surface is high enough to replenish some of the surface moisture and the product density continues to increase. This behavior was noticed by Litchfield and Okos (1992) during drying of pasta.

The physical texture of the dried product from rapid and slow drying techniques is very different. In rapid drying, the

dense crust formed initially may encourage expansion because internal vaporization is faster than transport out of the surface. This may cause subsequent porosity increase depending on the drying conditions (as in explosion puffing, for example). In slow drying, a dense product with uniform porosity forms. Depending on the end use, these products may be desirable/undesirable. If a long bowl life for a cereal product is required, a crusty product that prevents moisture reabsorption may be preferred. If a product with good rehydration capacity is required, the drying process below T_g may be preferred. Freeze-drying will be optimal for the latter purpose since little or no shrinkage occurs during drying.

From the preceding mechanistic analysis it may be suggested that collapse and the rate of drying play a major role in determining the moisture transport mechanism during drying. Over and above these factors, the mobility of water molecules in the matrix determined by the adsorption isotherms is an important property that determines the dryability of the matrix.

Mathematical development

The mathematical development starts with the modified Darcy's law of Achanta et al. (1994). This equation is used to model moisture flux (Achanta, 1995). The modified Darcy's law, assuming no solutes in the liquid phase, is

$$-\epsilon^w \underline{\nabla} p^w - \rho^w \epsilon^w \frac{\partial A^w}{\partial \epsilon^w} \underline{\nabla} \epsilon^w + \rho^w \epsilon^w \underline{g} = \underline{\underline{R}}_w^w \cdot \underline{v}^{w,s} \tag{1}$$

where ϵ^w is the volume fraction of the water phase; p^w is the pressure in the water phase; ρ^w is the density of the water phase; A^w is the Helmholtz free energy of the water phase; g is the acceleration due to gravity, $\underline{\underline{R}}_w^w$ is the resistivity tensor; and $\underline{v}^{w,s}$ is the water-phase velocity relative to the solid phase. The second term on the L.H.S. is defined as the "interaction potential." This term is not present in the traditional form of Darcy's law.

Achanta and Cushman (1994) showed that the interaction potential may be defined to be equal to the swelling pressure of the water phase. The nonequilibrium definition for the interaction potential is

$$\rho^w \epsilon^w \frac{\partial A^w}{\partial \epsilon^w} = p^w - p^s - \dot{\epsilon}^w \eta^m \tag{2}$$

where p^s is the solid-phase pressure; $\dot{\epsilon}^w$ represents the material derivative of the water-phase volume fraction with respect to the solid phase; and η^m represents the deformation viscosity. The swelling pressure, a multiphase counterpart of the single-phase osmotic pressure that drives liquid flow, is defined as

$$\Pi^w - \Pi^0 \equiv -\rho^w \epsilon^w \frac{\partial A^w}{\partial \epsilon^w} \tag{3}$$

This definition is modified from Achanta and Cushman (1994) to account for the fact that flow takes place from regions of low swelling pressure to regions of high swelling pressure. By definition, p^w, is the pressure in the liquid phase including all nonequilibrium contributions; and Π^w is an "equilibrium" system parameter that can be measured experimentally using a swelling-pressure experiment (Mokady and Low, 1968).

Substituting the swelling pressure definition Eq. 3 in Eq. 2,

$$-(\Pi^w - \Pi^0) = p^w - p^s - \dot{\epsilon}^w \eta^m \tag{4}$$

which upon rearrangement and on assuming $p^s \approx 0$ gives

$$p^w = (\Pi^0 - \Pi^w) + \dot{\epsilon}^w \eta^m \tag{5}$$

which shows that the pressure in the water phase equals the swelling pressure only at equilibrium. Traditional diffusion-based drying theories assume that the driving force for drying is the swelling pressure. But, as shown by the previous equation, this is only true at equilibrium and for a nonequilibrium flow situation, a pressure-based driving force (as opposed to a swelling-pressure-based driving force) is more appropriate.

Substituting Eq. 5 in Eq. 1:

$$-\epsilon^w \underline{\nabla}[(\Pi^0 - \Pi^w) + \dot{\epsilon}^w \eta^m] + (\Pi^w - \Pi^0) \underline{\nabla} \epsilon^w + \rho^w \epsilon^w \underline{g} = \underline{\underline{R}}_w^w \cdot \underline{v}^{w,s}. \tag{6}$$

Equation 6 can be rearranged to obtain

$$-\underline{\nabla}[(\Pi^0 - \Pi^w)\epsilon^w] - \epsilon^w \underline{\nabla}[\dot{\epsilon}^w \eta^m] + \rho^w \epsilon^w \underline{g} = \underline{\underline{R}}_w^w \cdot \underline{v}^{w,s} \tag{7}$$

Assuming that the resistivity tensor is isotropic and that gravity effects are negligible, Eq. 7 reduces to

$$\underline{v}^{w,s} = -\frac{K}{\eta^w}\left[\frac{d(\Pi^0 - \Pi^w)\epsilon^w}{d\epsilon^w} \underline{\nabla} \epsilon^w + \epsilon^w \underline{\nabla}(\dot{\epsilon}^w \eta^m)\right], \tag{8}$$

where K is the permeability of the material and η^w is the local viscosity of water in the material.

Equation 8 states that the moisture flux in the matrix is not only dependent on the moisture volume-fraction gradient but also on the rate at which the moisture volume-fraction changes. The rate of volume-fraction change is dependent on the matrix (or mixture) viscosity η^m which, as mentioned in the mechanistic description of drying, is a strong function of moisture and temperature of drying. For example, drastic changes in matrix viscosity close to T_g of the material [typically η^m changes by five orders of magnitude in the vicinity of T_g (Aklonis, 1983)] would affect the moisture transport mechanism in a significant fashion as indicated by the preceding flux equation.

The matrix equilibrium elasticity E is defined as

$$E \equiv -\frac{d(\Pi^w - \Pi^0)\epsilon^w}{d\epsilon^w}. \tag{9}$$

Physically this property of the matrix represents the change in swelling pressure (generalized variable: stress) with a change in volume fraction (generalized variable: strain). Hence E is a one-dimensional representation of the generalized elastic modulus of the material. To a first approxima-

tion, E may be assumed to be equal to the generalized elastic modulus of the material.

Substituting definition 9 in Eq. 8, we get

$$\underline{v}^{w,s} = -\frac{K}{\eta^w}[E\underline{\nabla}\epsilon^w + \epsilon^w\underline{\nabla}(\dot{\epsilon}^w\eta^m)]. \tag{10}$$

Equation 10 is modified Darcy's law in its simplified form. Before deriving the total water-mass balance, a cylindrical geometry is chosen for verification and Darcy's law is transformed to Lagrangian coordinates to simplify numerical analysis. The transformation equation used for this purpose is

$$\frac{\partial R}{\partial r} = \sqrt{1-\epsilon^w}, \tag{11}$$

where r represents the Eulerian radial coordinate, and R represents the Lagrangian radial coordinate assuming one-dimensional shrinkage.

The modified Darcy's law in Lagrangian coordinates can be shown as (Achanta, 1995):

$$v_R^{w,s} = -\frac{K}{\eta^w}\left[E\sqrt{1-\epsilon^w}\,\frac{\partial\epsilon^w}{\partial R} + \epsilon^w\sqrt{1-\epsilon^w}\,\frac{\partial}{\partial R}(\dot{\epsilon}^w\eta^m)\right]. \tag{12}$$

To express the moisture dependence of η^m, the mixture viscosity, an exponential model based on that of Thomas and Windle (1982) is used:

$$\eta^m = \eta_0^m\exp(-A\epsilon^w). \tag{13}$$

This model is empirical and is chosen because of its simplicity. Substituting the model for mixture viscosity in Eq. 13 and defining "effective" mixture properties, D, the "apparent diffusivity" and B, the "viscous deformation correction," as

$$D \equiv \frac{K}{\eta^w}\sqrt{1-\epsilon^w}\,E \tag{14}$$

$$B \equiv \frac{K}{\eta^w}\epsilon^w\sqrt{1-\epsilon^w}\,\eta_0^m = D\epsilon^w\frac{\eta_0^m}{E}, \tag{15}$$

the modified Darcy's law becomes

$$v_R^{w,s} = -D\frac{\partial\epsilon^w}{\partial R} - B\frac{\partial}{\partial R}(\dot{\epsilon}^w e^{-A\epsilon^w}). \tag{16}$$

Equation 16 is similar to the traditional diffusion equation in that water flux is proportional to moisture fraction gradient. The proportionality constant, D, however, is now defined in terms of matrix and solvent properties. This definition facilitates a study of the effect of fundamental structural and solvent property changes on the overall moisture diffusivity in the matrix.

Substituting Eq. 16 in the water-mass balance in Lagrangian coordinates, we get

$$\frac{\partial\epsilon^w}{\partial t} + \frac{(1-\epsilon^w)}{R}\frac{\partial}{\partial R}(R\epsilon^w v_R^{w,s}) = 0. \tag{17}$$

It can be shown that the total mass balance in terms of moisture gradient is

$$\frac{\partial\epsilon^w}{\partial t} = \frac{(1-\epsilon^w)}{R}\frac{\partial}{\partial R}\left(R\epsilon^w D\frac{\partial\epsilon^w}{\partial R}\right) + \frac{(1-\epsilon^w)}{R}\frac{\partial}{\partial R} \times\left[R\epsilon^w B\frac{\partial}{\partial R}\left(e^{-A\epsilon^w}\frac{\partial\epsilon^w}{\partial t}\right)\right]. \tag{18}$$

Nondimensionalizing Eq. 18 using the dimensionless parameters, we get

$$\bar{\epsilon}^w = \frac{\epsilon^w}{\epsilon_0^w} \tag{19}$$

$$\bar{R} = \frac{R}{R_0} \tag{20}$$

$$\theta = \frac{tD_0\epsilon_0^w}{R_0^2}, \tag{21}$$

where ϵ_0^w is the initial volume fraction of water; R_0, is the radius of the bone-dry solid; and D_0 is the apparent diffusivity at the initial volume fraction, that is, $D(\epsilon^w = \epsilon_0^w)$. It should be noted that D is a strong function of moisture content since permeability K is a strong function of moisture.

Also defining dimensionless functionals g and h as

$$g(\epsilon^w) = \bar{\epsilon}\frac{D}{D_0} \tag{22}$$

$$h(\epsilon^w) = \bar{\epsilon}^w\frac{B}{B_0}. \tag{23}$$

Substituting definitions 19–23 in Eq. 18,

$$\frac{\partial\bar{\epsilon}^w}{\partial\theta} = \frac{(1-\bar{\epsilon}^w\epsilon_0^w)}{\bar{R}}\frac{\partial}{\partial\bar{R}}\left(\bar{R}g\frac{\partial\bar{\epsilon}^w}{\partial\bar{R}}\right) + \frac{(1-\bar{\epsilon}^w\epsilon_0^w)}{\bar{R}}\frac{\partial}{\partial\bar{R}} \times\left[\bar{R}Deh\frac{\partial}{\partial\bar{R}}\left(e^{-A\bar{\epsilon}^w\epsilon_0^w}\frac{\partial\bar{\epsilon}^w}{\partial\theta}\right)\right], \tag{24}$$

where the Deborah number, De, is given by

$$De = \left(\frac{\epsilon_0^w\eta_0^m}{E}\right)\left(\frac{\epsilon_0^w D_0}{R_0^2}\right) = \frac{t_{\text{relax}}}{t_{\text{diffusion}}}. \tag{25}$$

Equation 24 is the overall moisture-transport equation that is applicable to both moisture-absorption and moisture-desorption problems. It is evident from Eq. 24 that at high Deborah numbers, the viscous relaxation of the matrix determines the rate of moisture desorption. In this regime, moisture transport in the material appears "non-Fickian" in the experimental time scale. At low Deborah numbers, however,

the relaxation processes are rapid and the second term on the R.H.S. of Eq. 24 is negligible. In this case, moisture transport appears "Fickian."

Application of the multiphase transport theory to drying

In application of the moisture-transport equation to the drying problem, it is assumed that heat transfer is rapid compared to mass transfer. As shown by Waananen (1991) for pasta, a typical biopolymer with high starch and protein content has thermal diffusivities much larger than mass diffusivities, and hence thermal gradients in the sample during drying may be neglected. Consequently, the heat-transport equation is neglected in further model development.

To apply Eq. 24 to a drying situation, initial and boundary conditions are needed. The initial condition is given by

$$\bar{\epsilon}^w = 1 \quad \text{at} \quad \theta = 0 \forall r. \tag{26}$$

The boundary condition at the center of the cylinder, by symmetry, is

$$\frac{\partial \bar{\epsilon}^w}{\partial \bar{R}} = 0 \quad \text{at} \quad \bar{R} = 0 \quad \text{for} \quad \theta > 0. \tag{27}$$

The boundary condition at the surface $r = R_0$ assuming the moisture flux to the surface from the interior is equal to the rate of vaporization from the surface:

$$\frac{1}{Bi} g \frac{\partial \bar{\epsilon}^w}{\partial \bar{R}} + \frac{1}{Se} h \frac{\partial}{\partial \bar{R}} \left(e^{-A \bar{\epsilon}^w \epsilon_0^w} \frac{\partial \bar{\epsilon}^w}{\partial \theta} \right) = X^\star - a_w$$

$$\text{at} \quad \bar{R} = 1 \quad \text{for} \quad \theta > 0, \tag{28}$$

where Bi is the Biot number given by:

$$Bi = \frac{k'_G R_0}{D_0 \epsilon_0^w} = \left(\frac{R_0^2}{D_0 \epsilon_0^w} \right) \Big/ \left(\frac{R_0}{k'_G} \right) \tag{29}$$

and Se is the Shell number defined as

$$Se = \frac{Bi}{De}; \tag{30}$$

k'_G is the external mass transfer coefficient; a_w is the water activity at the surface; and $X^\star$ is the external relative humidity.

The Shell number accounts for the characteristic time scales of evaporation, diffusion, and relaxation processes. When the time scales of these three processes are comparable, the Shell number plays a significant role in determining the surface drying rate. For example, when Bi is $\gg 1$ and De is ≈ 1 (i.e., the material is close to undergoing a glassy transition during drying), the surface drying rate is influenced equally by Bi and Se. It is clear that the surface moisture is time and relaxation-rate dependent under these conditions. In contrast, since conventional drying theories take only Bi into account, they assume that the surface reaches equilibrium moisture under these conditions.

The surface boundary condition Eq. 28 determines the rate at which the surface reaches equilibrium with the external environment. In the conventional polymer-science literature (Wu and Peppas, 1993) the surface of the material is assumed to reach a solvent content that is almost instantaneously in equilibrium with external conditions. However, as shown in Eq. 28, this equilibration process may be time dependent as determined by the Shell number.

To conduct a sensitivity study on the role of various matrix and solvent parameters on the drying behavior of the material, and to compare model predictions with experimental data, an implicit finite difference scheme based on the algorithm proposed by Wu and Peppas (1993) was developed.

Materials and Methods

Experimental verification of the proposed drying model involves: (1) measurement of mixture properties that serve as inputs to the model; for example, solvent viscosity in the matrix (or alternatively solvent self-diffusion coefficient in the matrix), matrix viscosity at different moistures and temperatures, and adsorption isotherms at different temperatures; (2) measurement of drying kinetics of the matrix at different temperatures; and (3) comparison of the predictions of the drying model with experimental data to assess the validity of the model.

Material preparation

A food biopolymer system containing starch and gluten was chosen for the experimental study. The ratio of starch to gluten was chosen to be 4:1 so that the material is representative of a typical food material. Gels of high moisture content were prepared by adding water in the required ratio to a mixture of corn starch and wheat gluten (Sigma Chemical Corp.), heating the solution above 80°C to gel, and moulding the gels using aluminum moulds. Low-moisture gels were prepared by allowing the moulded high-moisture gels to desorb moisture over salt solutions. Moisture content of the material was measured gravimetrically by drying the wet material at 130°C for longer than 4 h.

Desorption Isotherm Experiments. Desorption isotherms were measured by storing the gels over salt solutions at different temperatures and by measuring the moisture content of the gels after equilibrium was assumed to have been achieved. Sample weight was measured periodically, and when no significant sample weight change was noticed for three consecutive days equilibrium was assumed to have been reached.

Self-Diffusion Experiments. The self-diffusion coefficient of moisture in the gel was measured using tritiated water as a radioactive tracer. Four diffusion cells based on the designs of Mokady and Low (1968) and Axelsson et al. (1991) were constructed and self-diffusion coefficients were calculated from the flux of tracer measured using a Tricarb Liquid Scintillation Counter.

Mechanical Property Experiments. A two-point bending test following the procedures of Kim (1994) was used to characterize the mechanical properties of samples at various moistures, and to determine the glass-transition temperature of the material. Flexure tests were conducted with a Sintech material-testing machine using a simple beam-bending technique.

Drying Experiments. Drying experiments were conducted based on the procedures of Waananen (1989). A Cahn 1000 electronic balance connected to a data-acquisition system was used to monitor the weight change of the sample with time during drying.

Results and Discussion

Initially a qualitative and quantitative analysis of drying behaviors (moisture profiles in the material and drying kinetics) under different conditions is conducted based on the proposed model. The predictions of the model are compared with expected drying behaviors. Second, the drying model is verified by applying it to drying experiments and by comparing its predictions with experimental drying kinetics. The finite difference scheme proposed earlier is used for predicting the drying behavior.

Analysis of the effect of Deborah and Biot numbers

The simulation studies are structured to present the effect of Deborah and Biot numbers on drying. Traditionally, only the effect of the Biot number is considered significant. But for shrinking viscoelastic polymers, the Deborah number also plays a significant role in determining the drying mechanism.

Numerical simulations of drying were conducted by solving Eq. 24 using the initial condition, Eq. 26, and the boundary conditions, Eqs. 27 and 28. The equations were first solved in the Lagrangian frame and then converted back to the Eulerian frame using Eq. 11. An implicit finite difference scheme was developed based on the method of Wu and Peppas (1993). The numerical procedure was shown to be convergent for limiting cases (Achanta, 1995).

The simulation results are presented in Figures 1–5 and the parameters fixed in the simulations are presented in Table 1. A diffusivity of 6.0×10^{-10} m^2/s, viscosity, η_0^m, of 1.0×10^{12} Pa·s, A, of 10, and external relative humidity, $X^\star$, of 0.02 were used for these simulations. In Figure 1 moisture content is plotted as a function of (drying time)$^{1/2}$ since Fickian and non-Fickian effects can be clearly distinguished in such a plot. From Figure 1 it is evident that at high Biot and low Deborah numbers the drying curve is initially linear and that the drying curve levels off only when equilibrium is reached. However, at low Biot numbers, the drying curve exhibits a sigmoidal nature that indicates that the drying curve is not only a function of the Deborah number but also the shell, Se, number.

At medium Deborah numbers the mixture relaxation time is comparable to the moisture diffusion time. Moisture transport in this regime is expected to be non-Fickian. Figure 2 presents moisture curves during medium Deborah number drying for three Biot numbers: 52, 3.4, and 103, respectively.

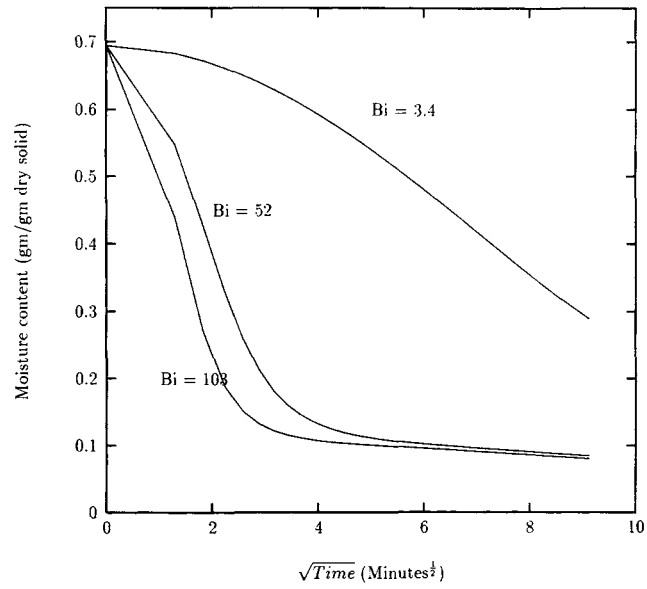

Figure 2. Effect of *Bi* on medium *De* drying curves.

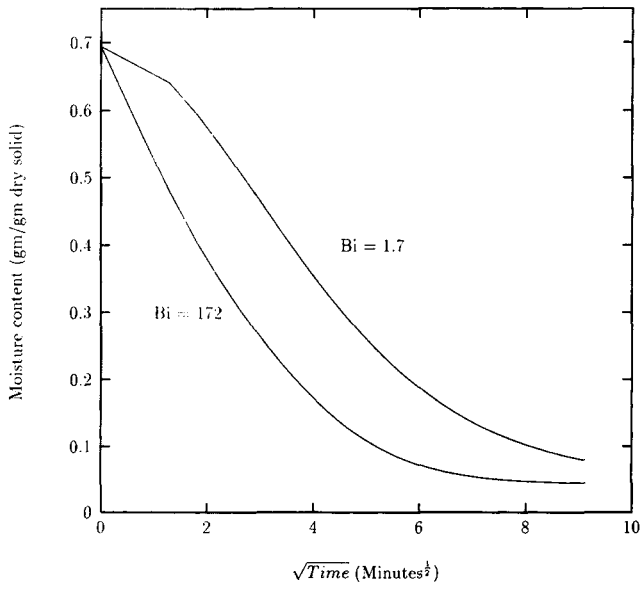

Figure 1. Comparison of low *De* drying curves at low and high *Bi*.

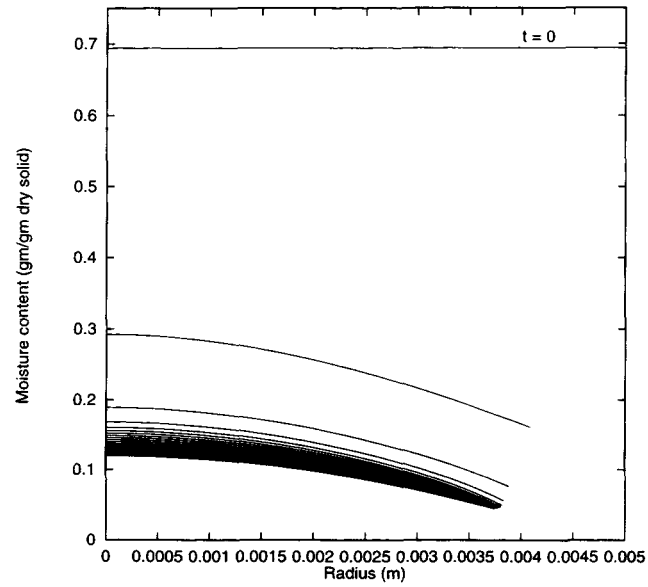

Figure 3. Medium *De* moisture profiles (time step = 250 s, De = 33.1, *Bi* = 103).

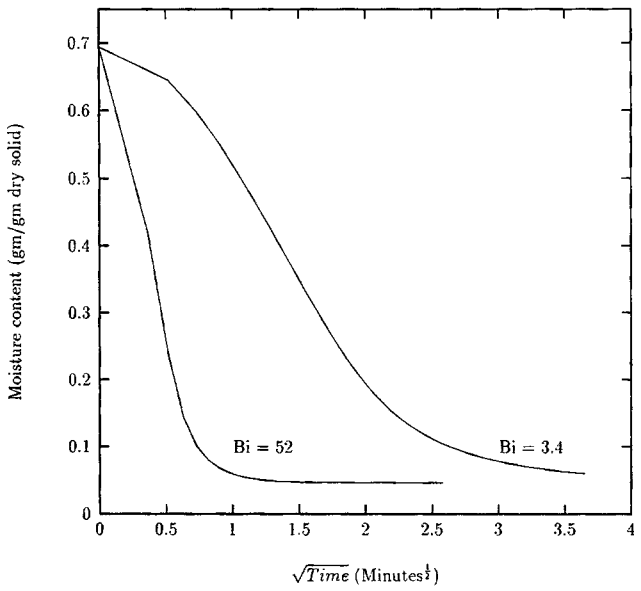

Figure 4. Effect of *Bi* on high *De* drying curves.

It is evident from Figure 3 that at medium Deborah and high Biot numbers, the moisture profiles are pseudouniform initially because of the low viscosity of the material (the changing outer radius in Figure 3 indicates sample shrinkage during drying). However, during the later stages of drying, when the surface of the material reaches the equilibrium moisture, a moisture gradient develops and drying practically "shuts off." This behavior is typical of the formation of a crust during drying.

At high Deborah numbers, the relaxation time of the mixture is much larger than the moisture-diffusion time. As a result, the mixture viscosity plays a significant role in determining the rate at which drying proceeds. Figure 4 presents moisture curves during high Deborah number drying for two

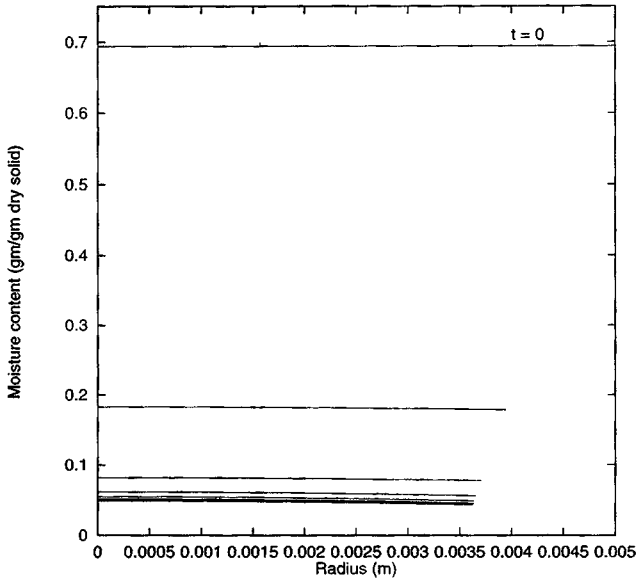

Figure 5. High *De* moisture profiles (time step = 20 s, *De* = 994, *Bi* = 52).

Table 1. Parameters Fixed in the Simulation Studies

Parameter	Model/Value
Radius	0.005
ρ_s/ρ_w	1.5
X^*	0.02
E	$10^5/(\epsilon^w)^2$
A	10.00
a_w	$X^{1/0.38}/(X^{1/0.38}+C^{1/0.38})$

Biot numbers: 52 and 3.4, respectively. A diffusivity of 1.8×10^{-8} m^2/s; viscosity η_0^m of 1.0×10^{12} Pa·s, A of 10; and external relative humidity, X^*, of 0.02 were used for these simulations. It is evident from Figure 5 that for high Deborah number drying, moisture profiles are flatter compared to medium Deborah number drying because diffusion times are very short. Drying is almost entirely surface driven, and when the material surface reaches the equilibrium moisture, drying shuts off.

Verification of the drying model

To verify the proposed drying model with a biopolymer, properties of the material were determined independently and were substituted in the drying model. The model predictions were then compared with experimental drying curves to evaluate the validity and the limitations of the model.

Verification of the Shrinkage Hypothesis. One-dimensional shrinkage (in the radial direction) in a long gel cylinder with loss in moisture can be verified by plotting the radius of the gel as a function of moisture content. If shrinkage in the material is equal to the amount of moisture lost, the following equation is valid:

$$\frac{V}{V_0}=\left(\frac{r}{r_0}\right)^2=\left(\frac{1}{1+X_0\dfrac{\rho_s}{\rho_w}}\right)+\left(\frac{1+X}{X_0+\dfrac{\rho_w}{\rho_s}}\right), \qquad (31)$$

where V is the volume of the cylinder at any moisture; V_0 is the initial volume; r is the radius of the gel at any moisture; r_0 is the initial radius; and X_0 is the initial moisture content of the gel.

Based on the previous equation, a plot of $(r/r_0)^2$ as a function of X should be a straight line. Gels of diameter 1.0 cm were dried at room temperature to different moistures, and the change in the radius with moisture content was noted. The data are plotted in Figure 6. As can be seen from the figure, at high moistures shrinkage is proportional to moisture lost. The slope of the curve was determined to be 0.37 ($R^2 = 0.96$), from which ρ_s/ρ_w was calculated to be 1.05.

As moistures below 0.6 g/g dry solid, however, shrinkage is not proportional to volume lost. It is probable that the material starts transforming to a glassy matrix around this moisture and shrinkage slows down as a result. Macropores inside the material may be forming below this moisture content.

To test whether in fact the material transforms to a glassy matrix at moistures below 0.6 g/g dry solid, the bending modulus of the material was measured at different moistures as a function of temperature. The data at 26°C, 40°C, and 55°C

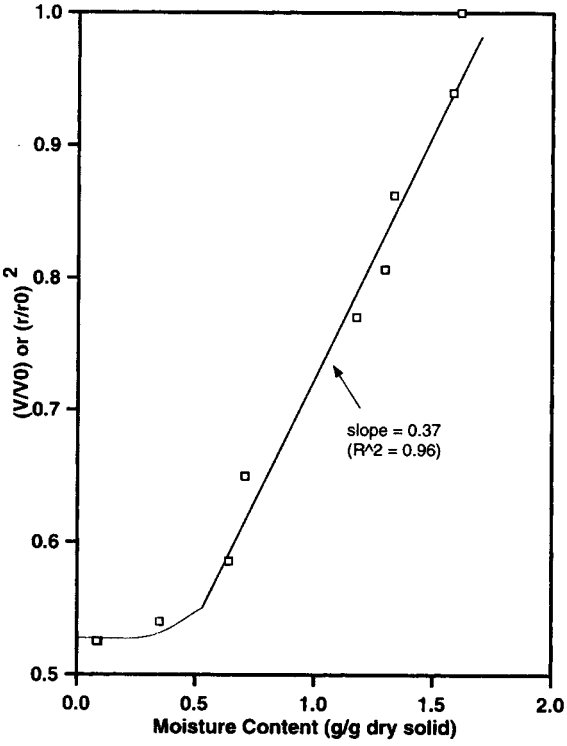

Figure 6. Shrinkage in starch–gluten gels during drying.

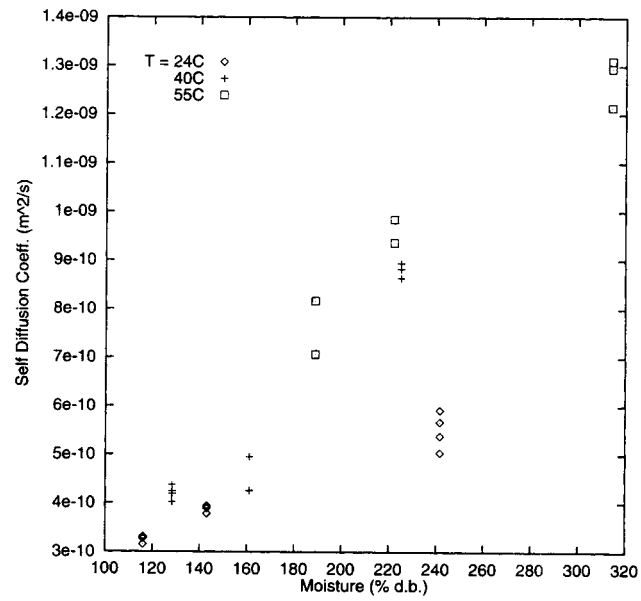

Figure 8. Self-diffusion coefficients of moisture in starch–gluten gels.

are summarized later in Figure 9. It is evident from the data that the bending modulus starts increasing exponentially as moisture content decreases below 0.6 g/g dry solid, the same moisture at which shrinkage during drying slows down.

The bending data, however, do not show any clear difference between moduli at the same moisture but different temperatures. This is probably due to large experimental errors noticed at intermediate and low moisture using the bending test. However, no further error analysis was conducted because the primary purpose of the bending tests was to determine the slope of the bending curve and to identify the point at which glass transition occurs.

Determination of Matrix and Solvent Properties. The properties that serve as inputs to the drying model are isotherms, self-diffusion coefficient (D_{self}), parameter A, elasticity, viscosity and material permeability. Isotherms D_{self} and A were determined experimentally as a function of moisture content and temperature. Elasticity and viscosity were assigned models and values based on literature data and experimental

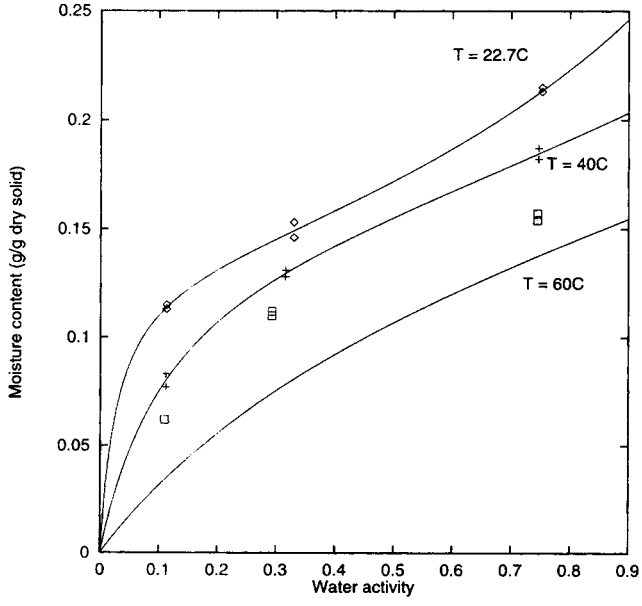

Figure 7. Starch–gluten isotherms at different temperatures.

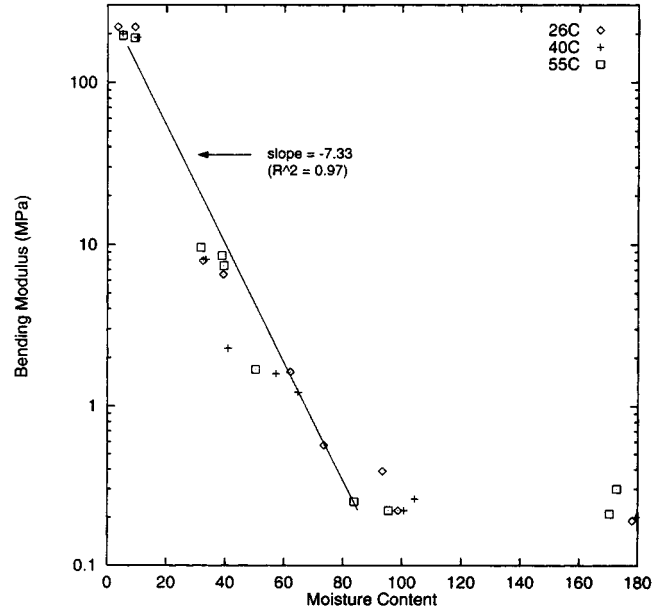

Figure 9. Determination of parameter *A* from bending data.

Table 2. GAB Equation Parameters for Starch-Gluten Gels (25°C–60°C)

Parameter	Model and Value
X_m	$1.91 \exp(-6.57/RT)$
C	$1.21\times10^{-6} \exp(43.89/RT)$
K	$2.36\times10^{-4} \exp(18.95/RT)$

bending data, while permeability as a function of moisture was determined empirically from the drying data.

Determination of Desorption Isotherms. The isotherms data for the starch–gluten gels at different temperatures are presented in Figure 7. The GAB equation (Van den Berg, 1981) of the following form was fitted to these data:

$$\frac{X}{X_m} = \frac{CKa_w}{(1-Ka_w)(1-Ka_w+CKa_w)}, \tag{32}$$

where X_m is the monolayer moisture content, and C and K are semiempirical parameters. These parameters are temperature dependent following the Arrhenius equation. The parameter values determined using SAS NLIN (SAS Institute) are presented in Table 2.

From Figure 7 it may be seen that the isotherm fits experimental data at 22.7°C and 40°C. At 60°C the isotherm underpredicts the equilibrium moisture. This may be partially due to the fact that there are too few data points to fit the GAB isotherm.

Determination of Moisture Self-Diffusion Coefficients. The local viscosity of water in the matrix η^w determines the moisture mobility in the matrix as shown by Eq. 14. η^w is inversely related to the self-diffusion coefficient of water in the gel as given by the Stokes–Einstein equation:

$$D_{\text{self}} = \frac{\beta c_i T}{\eta^w}, \tag{33}$$

where β is a constant related to the tortuosity of the gel and c_i is a constant related to the radius of the water molecule.

The self-diffusion data obtained from the starch–gluten gels at different moistures and temperatures and presented in Figure 8. As is evident from the data, the self-diffusion coefficient of moisture in gels increases as moisture increases at all three temperatures. The data obtained are comparable in magnitude to those determined for starch–gluten gels using NMR (Umbach et al., 1992). For determining the activation energy for self-diffusion, average self-diffusion coefficients at each temperature were calculated and fit to the Arrhenius equation:

$$D_{\text{self}} = D_0 \exp(-E_a/RT) \tag{34}$$

where E_a is the activation energy and D_0 is a constant. The model was fit using a regression model. The best fit values determined were $D_0 = 4.2\times10^{-6}$ m^2/s, and $E_a = 22.5$ kJ/mol·K.

Determination of Viscosity Model Parameters. The viscosity and elasticity models used for verification of the drying model are

$$\eta^m = \eta_0^m \exp(-A\epsilon^w) \tag{35}$$

$$E = E_0 \exp(-A\epsilon^w). \tag{36}$$

The viscosity model Eq. 35 is similar to that proposed by Thomas and Windle (1982), while the proposed elasticity model Eq. 36 is an extension of the viscosity model based on the hypothesis that elasticity and viscosity behave as similar moisture functionals close to the glass-transition temperature. This is an extension of the idea behind the Williams–Landel–Ferry equation (Aklonis, 1983). Based on the preceding hypothesis, A was determined empirically by fitting the log (bending modulus) data below a moisture content of 80% to a straight line. The slope of the straight line at low moistures determined using linear regression was -7.33 with an $R^2 = 0.97$. The low moisture fit and the experimental data are presented in Figure 9. To account for the fact that A is 7.33 at low moistures, and that it decreases as moisture content increases, a simple linear model of the following form was chosen:

$$A = 7.33 - 5.0\epsilon^w. \tag{37}$$

This equation suggests that at high moistures, A approaches a limit of 2.33, the approximate slope of the log (bending modulus) curve at high moistures. η_0^m was assumed to be equal to 2.0×10^{12} Pa·s at 21.5°C and 0.5×10^{12} Pa·s at 40°C based on viscosity data published for glassy flood materials (Levine and Slade, 1991), and E_0 was assumed to be 1.0×10^8 Pa based on elasticity data published for glassy foods (Levine and Slade, 1991).

"Effective" Diffusivity Model. The apparent diffusivity in terms of its components is given by Eq. 14:

$$D = \frac{K}{\eta^w}\sqrt{1-\epsilon^w}\,E.$$

Since $1/\eta^w$ is proportional to D_{self}, Eq. 14 can be rewritten as

$$D = K' D_{\text{self}} \sqrt{1-\epsilon^w}\,E, \tag{38}$$

where the K' parameter is moisture dependent and D_{self} is assumed to be only temperature dependent. The moisture dependence of D_{self} is assumed to have been absorbed by K'. The previous equation for D may be considered as a bifunctional equation in that the temperature dependence of D arises from the temperature dependence of D_{self}, and the moisture dependence of D arises from K' and E (assuming E does not vary to a great degree in the temperature range of interest).

Using Eq. 36, it can be shown that Eq. 38 can be reduced to (Achanta, 1995):

$$D = D_{\text{self}}(\epsilon^w). \tag{39}$$

Incorporating the equation for D_{self} in Eq. 62, the final apparent diffusivity model is

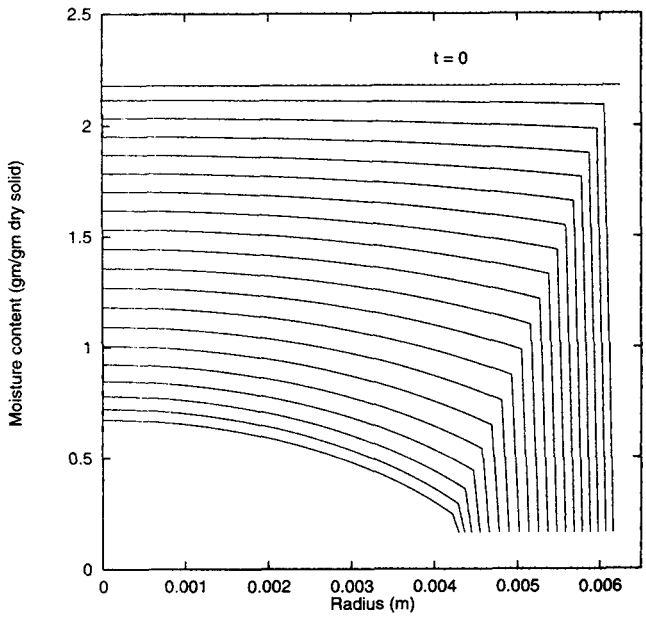

Figure 10. Predicted moisture profiles (time step = 3,000 s, *De* = 36.1, *Bi* = 11.4e4, *T* = 21.5°C).

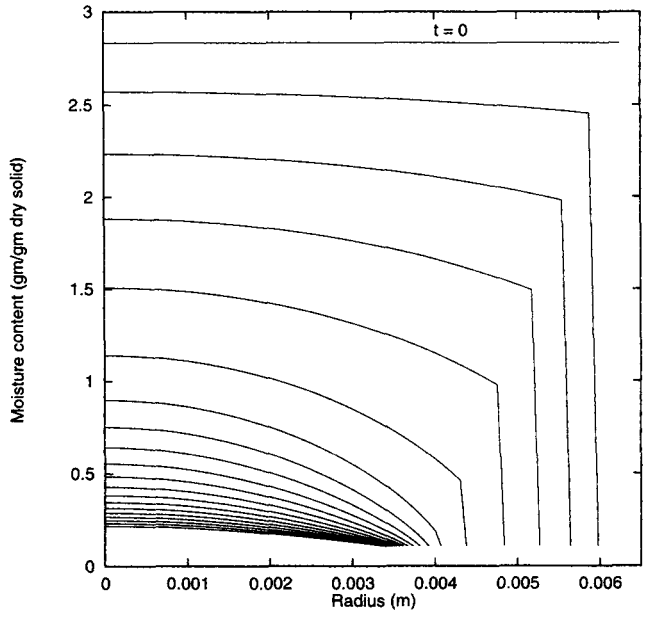

Figure 12. Predicted moisture profiles (time step = 3,000 s, *De* = 34.4, *Bi* = 5.2e4, *T* = 40°C).

$$D = 4.2\times10^{-6}\exp(-22.85/RT)(\epsilon^{w}), \qquad (40)$$

where R is 8.314×10^{-3} kJ/mol·K.

Knowing D, B can be determined from Eq. 15 based on the model postulated for E earlier. Knowing D and B, Eq. 18 can be solved to predict moisture profiles and drying curves for the gels.

Comparison of Model Predictions with Drying Data. The drying model proposed earlier, incorporating all the property models, was solved using a finite difference C-program. This program assumes that the boundary of the gel reaches equilibrium because of the high Biot numbers (of the order of 10^4) at which the drying experiments were conducted. Drying experiments at two different drying temperatures of 21.5°C and 40°C were conducted to verify the model. Figures 10 and 11 present predicted drying curves and moisture profiles at 21.5°C and compare the drying curves with experimental data. Figures 12 and 13 present predicted drying curves and moisture profiles at 40.0°C and compare the drying curves with experimental data. The drying curves at both temperatures exhibit sigmoid shapes typical of non-Fickian diffusion. On comparison of the drying curve data with predictions, it can be concluded that the model captures the essential sigmoidal shape of the drying curves at both temperatures. The model

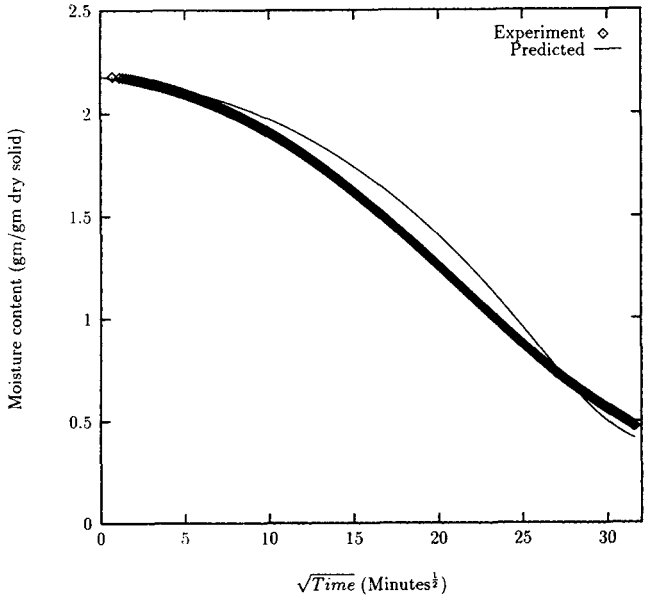

Figure 11. Comparison of predicted and experimental drying curves at 21.5°C.

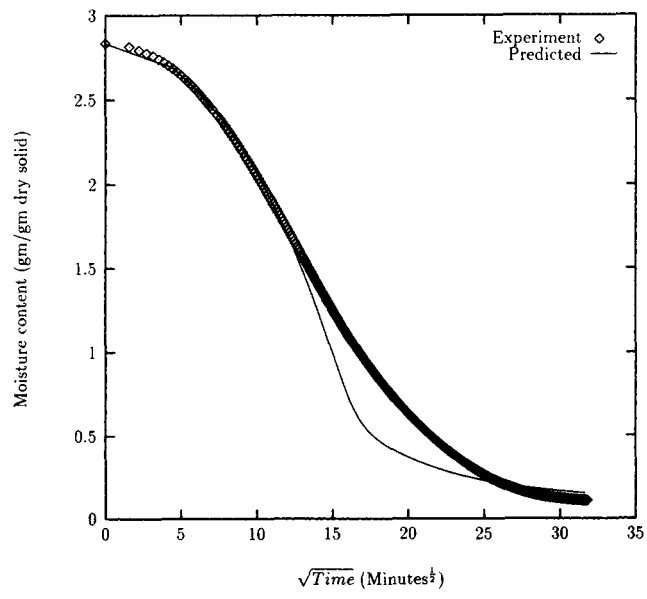

Figure 13. Comparison of predicted and experimental drying curves at 40°C.

predictions agree reasonably well with experimental data at both temperatures.

The moisture profiles presented show that a skin front develops during drying of the gels. This is typical of glassy transition in the material during drying. The slope of the front is constant in the initial periods of drying. However, as seen from the predictions, the slope of the front decreases (or the front curves in) as drying proceeds. This implies that as drying proceeds, the impermeable skin on the gel grows. Also, as shown in Figure 12, the skin disappears after approximately 256 min of drying (approximately 16 $\text{min}^{0.5}$ where drying slows down dramatically, as shown in Figure 13). This is indicative of the fact that the whole material becomes glassy at this stage. The data of Schrader and Litchfield (1992) during drying of model gels support the model predictions qualitatively.

Conclusions

A new mechanistic and mathematical drying model was developed that accounts for time-dependent shrinkage in biopolymers. The drying model is valid for high-moisture drying of biopolymers where shrinkage compensates for moisture lost, and moisture transport is predominantly in the liquid phase. Dimensional analysis of the moisture transport equation revealed that both the Deborah and the Biot numbers determine the shapes of the moisture profiles in the material during drying. Dimensional analysis of the surface-drying boundary condition revealed that the Shell number determines the rate at which the surface achieves equilibrium during drying. The drying model was verified by comparing simulation results with experimental data from drying of starch–gluten gels of high moisture. The moisture profiles predicted by the drying model show a skin front that spreads into the material as drying proceeds.

Acknowledgments

The authors thank the Army Research Office (Contract DAAL03-90-G-0074), the U.S. Department of Agriculture (Contract 94-37500-0052), and the National Science Foundation (Contract 95-10066-BES) for partial support of this project.

Notation

g = dimensionless functional of space and time describing the moisture dependence of the diffusion coefficient
h = dimensionless functional of space and time describing the moisture dependence of the shrinkage correction
P_w = water-vapor pressure, Pa
P_w^0 = saturated water-vapor pressure, Pa
R = universal gas constant 8.314, J/mol·K
R = material radius, m
$\bar{R}$ = normalized material radius
r = spatial radius
T = temperature, K
T_g = glass-transition temperature, K
t = time, s
X = moisture content, kg water/kg dry solid
X_{cr} = critical moisture content, kg water/kg dry solid
X_e = equilibrium moisture content, kg water/kg dry solid

Greek letters

$\bar{\epsilon}$ = normalized volume fraction
ρ_s = density of solid, kg/m^3
ρ_w = density of water, kg/m^3
θ = dimensionless time

Literature Cited

Achanta, S., "Moisture Transport in Shrinking Gels during Drying," PhD Thesis, Purdue Univ., West Lafayette, IN (1995).
Achanta, S., and J. H. Cushman, "Non-Equilibrium Swelling and Capillary Pressure Relations for Colloidal Systems," *J. Colloid Interface Sci.*, **168,** 266 (1994).
Achanta, S., J. H. Cushman, and M. R. Okos, "On Multicomponent, Multiphase Thermomechanics with Interfaces," *Int. J. Eng. Sci.*, **32,** 1717 (1994).
Aklonis, J. J., *Introduction to Polymer Viscoelasticity*, Wiley, New York (1983).
Axelsson, A., B. Westrin, and D. Lloyd, "Application of the Diffusion Cell for the Measurement of Diffusion in Gels," *Chem. Eng. Sci.*, **46,** 913 (1991).
Crapiste, G. H., S. Whitaker, and E. Rotstein, *Drying* '85, R. Toei and A. S. Mujumdar, eds., Hemisphere, New York (1985).
Ferry, J. D., "Viscoelastic Properties of Polymers," Wiley, New York (1980).
Jomaa, W., and J. R. Puiggali, "Drying of Shrinking Materials: Modeling with Shrinkage Velocity," *Drying Technol.*, **9,** 1271 (1991).
Karathanos, V., S. Anglea, and M. Karel, "Collapse of Structure During Drying of Celery," *Drying Techn.*, **11,** 1005 (1993).
Ketelaars, A. A. J., W. Jomaa, J. R. Puiggali, and W. J. Coumans, "*During* '92," A. S. Mujumdar, ed., Elsevier, Amsterdam (1992).
Kim, M., "Linear Hygrothermal Stress Development in Food Products during Simultaneous Heat and Mass Transfer Process," PhD Thesis, Purdue Univ., West Lafayette, IN (1994).
Kishimoto, A., H. Fujita, H. Odani, M. Kurata, and M. Tamura, "Successive Differential Absorptions of Vapors by Glassy Polymers," *J. Phys. Chem.*, **64,** 594 (1960).
Lartigue, C. J. R. Puiggali, and M. Quintard, *Drying* '89, A. S. Mujumdar and M. Roques, eds., Hemisphere, New York (1989).
Levine, H., and L. Slade, *Water Relationships in Foods: Advances in 1980s and Trends for the 1990s*, Plenum Press, New York (1991).
Litchfield, J. B., and M. R. Okos, "Moisture Diffusivity in Pasta during Drying," *J. Food Eng.*, **17,** 117 (1992).
Mokady, R. S., and P. F. Low, "Simultaneous Transport of Water and Salt Through Clays: I. Transport Mechanisms," *Soil Sci.*, **102,** 112 (1968).
Peppas, N. A., and R. W. Korsmeyer, *Hydrogels in Medicine and Pharmacy*, Vol. III, N. A. Peppas, ed., CRC Press, Boca Raton, FL (1987).
Schrader, G. W., and J. B. Litchfield, "Moisture Profiles in a Model Food Gel during Drying: Measurement Using Magnetic Resonance Imaging and Evaluation of the Fickian Model," *Drying Technol.*, **10,** 295 (1992).
Suarez, C., and P. E. Viollaz, "Shrinkage Effect on Drying Behavior of Potato Slabs," *J. Food Eng.*, **13,** 103 (1991).
Thomas, N. L., and A. H. Windle, "A Theory of Case-II Diffusion," *Polymer*, **23,** 529 (1982).
Umbach, S. L., E. A. Davis, J. Gordon, and P. T. Callaghan, "Water Self Diffusion Coefficients and Dielectric Properties Determined for Starch-Gluten-Water Mixtures Heated by Microwave and by Conventional Methods," *Cereal Chem.*, **69,** 637 (1992).
Van Den Berg, C., "Vapor Sorption Equilibria and Other Water-Starch Interactions: A Physico-Chemical Approach," PhD Thesis, Wageningen University, The Netherlands (1981).
Viollaz, P., "An Analytical Solution for Diffusion in a Shrinking Body," *J. Poly. Sci.: Poly. Phys. Ed.*, **23,** 143 (1985).
Waananen, K. M., "Analysis of Mass Transfer Mechanisms during Drying of Extruded Pasta," PhD Thesis, Purdue Univ., West Lafayette, IN (1989).
Waananen, K. M., and M. R. Okos, "Analysis of Bulk Flow Transfer," *Technol. Today*, **5,** 289 (1991).
Whitaker, S., *Advances in Drying*, A. S. Mujumdar, ed., Hemisphere, New York, Vol. I, 5: 289–296 (1980).
Wu, J. C., and N. A. Peppas, "Numerical Simulation of Anomalous Penetrant Diffusion in Polymers," *J. Appl. Poly. Sci.*, **49,** 1845 (1993).

Manuscript received May 6, 1996, and revision received Mar. 7, 1997.